

# Future Radiation Damage in Space Due to the South Atlantic Anomaly

J. R. Heirtzler\*

*Laboratory for Terrestrial Physics, NASA/Goddard Space Flight Center  
Greenbelt, MD 20771*

---

## Abstract

The geographic limits of the South Atlantic Anomaly, as defined by radiation damage, are compared to contours of geomagnetic total field intensity, as defined by the 1995 IGRF, for the present and recent past. The most likely secular variation of the geomagnetic field is estimated and used to extrapolate the geomagnetic field to the year 2100. This indicates that radiation damage to spacecraft and humans in space will likely increase and to cover a much larger geographic area.

---

## 1. Introduction

In order to understand what might be the future radiation hazard of the South Atlantic Anomaly it will be necessary to briefly review how the geomagnetic field is related to the radiation hazard in Low Earth Orbit at the present time. It has been known for more than 40 years that there is a weak geomagnetic field in the South Atlantic Ocean, known as the South Atlantic Anomaly (SAA). It is especially important to the radiation environment near the Earth. This area of intense radiation causes damage to the many spacecraft in Low Earth Orbit and is a hazard to astronauts/cosmonauts which are there. The basic physical laws governing charged particle motion in the geomagnetic field are well understood, although significant questions remain about the density of charged particles and how they vary with time.

Of the three well known types of charged particle motion in the

---

\*Fax: 301-614-6015

Email: [jamesh@ltpmail.gsfc.nasa.gov](mailto:jamesh@ltpmail.gsfc.nasa.gov)

---

geomagnetic field (gyrorotation about the geomagnetic line of force, the bounce of the particles from hemisphere to hemisphere, with mirror points in each hemisphere and the drift of particles to the east or west because of the longitudinal variation of field strength) only the bounce motion will be considered here. It is the lower mirror points over the SAA that is generally thought responsible for the more intense radiation there, because, there is more interaction with the atmosphere there. We will examine this point in detail, looking at the configuration of the geomagnetic field and the places where radiation damage occurs.

## 2. Configuration of the Geomagnetic Field

We need only consider the total intensity of the field rather than its directional components, although for ray tracing one needs to use the declination and inclination of the geomagnetic field vector. For considering the present field we will use the International Geomagnetic Reference Field for 1995 (IGRF 95), where the spherical harmonic coefficients and their first time derivatives are given by Barton, C.E., et al. (1996). IGRF 95 was used as an input to a computer subroutine to give the components and total field at any latitude, longitude, altitude, and time. This data was used to graphically display various aspects of the field.

Figure 1 is a contour plot of the total field for the year 1995.0 at the Earth's surface. It shows the SAA, which has a minimum value of about 23,000 nT located about 700 km inland from the coast of Southern Brazil. Also shown are the highs in the Canadian Arctic, Siberia, and in Antarctica south of Australia. The SAA is generally said to be due to the fact that the inclined dipole axis of the Earth is displaced in the direction of the northwest Pacific (21.47 N, 144.77 E) by 527 km. In fact when the geomagnetic field of the Earth is plotted using only the inclined, offset axis terms, the low in the South Atlantic is somewhat differently shaped from the SAA shown in Figure 1, indicating that the SAA has a contribution from the higher order terms of the IGRF.

Contrary to common approximations the geomagnetic field near the Earth differs significantly from that of a dipole. Contour plots of the total field were made at altitudes of 200 km, 500 km, 1000 km, and 5000 km. It is only at 5000 km (0.78 Earth radii) that the contours of field strength resemble those of

the inclined offset dipole. At 10,000 km the field strength is reduced to about one-tenth its surface value. At 15,000 km (2.35 Earth radii) the field resembles that of an inclined axial dipole.

The SAA greatly influences the shape of the geomagnetic field lines. A ray tracing program, using the IGRF 95, was written and used to show geomagnetic field lines. To illustrate the asymmetry of the geomagnetic field lines Figure 2 shows field lines which originate at latitudes 20 S, 40 S, and 60 S along the longitudes 40 W and 140 E. 40W is near the longitude of the SAA and 140 E is near the longitude of the Siberian and Antarctic highs. These two longitudes are separated by 180 degrees. Notice that the line which leaves 60 S terminates near 80 N along 140 E, but at about 40 N along 40 W. As the Earth rotates during the course of a day this asymmetric field creates a changing, magnetically complex region in near space.

The ray tracing program which generated field values along a line of force was used to locate the magnetic equator, where the dip angle changed sign, in order to determine the value of the equatorial field value there. Knowing this field value ( $B_e$ ) one can calculate the field value for the mirror point ( $B_m$ ) for any equatorial pitch angle ( $\Phi_e$ ) by the relationship

$$B_e / \sin^2(\Phi_e) = B_m / \sin^2(\Phi_m) = B_m \quad \text{Eq.(1)}$$

since the mirror point pitch angle  $\Phi_m = 90$  degrees. This value of  $B_m$  allows one to determine the position of the mirror point along the line of force.

Figure 3 displays three lines of force starting at latitudes 40 S, 30 S, and 20 S, all along longitude 60 W. Points and numbers along each field line show the mirror points for different equatorial pitch angles. Heights below about 100 km altitude are invalid because the atmosphere extends upwards to about this altitude and particles of the radiation are scattered or absorbed there. The line which originates at 20 S is almost totally within the atmosphere and has few particles associated with it.

A consideration of the line which starts at 40 S illustrates that particles with equatorial pitch angles of less than about 45 degrees (loss cone 45 degrees) are removed from the southern end of the line, invalidating mirror points of less than this pitch angle on the northern end of the line. This same asymmetry is true on the other lines because of the low value of the SAA.

In considering how these mirror points might be related to the intensity of radiation in space one should be aware of how the number density of particles varies as a function of equatorial pitch angle. This is characterized by the anisotropy index  $n$  in the equation for the distribution function  $J(\Phi)$

$$J(\Phi) = J \sin^n(\Phi) \quad \text{Eq.(2)}$$

Where  $J$  is the value of  $J(\Phi)$  when  $\Phi = 90$  degrees.

Fung (1996) has shown that, for electrons and protons,  $n$  has values of 1 to 10, with the larger values more common. The relative probability  $J(\Phi)/J$  is large, especially for larger values of  $n$ . This shows that most particles have high equatorial pitch angles, nearing 90 degrees. Thus most particles will be mirroring near the top of their field line trajectory, and relatively fewer particles will reach the atmosphere. This more intense radiation near the equator has not been explicitly reported in the literature.

### 3. Damage in Low Earth Orbit

It is convenient to first look at the damage to spacecraft and then to look at the radiation hazard to humans. Although it is difficult to characterize any space mission as typical it is instructive to briefly consider well-documented cases of each of these two types of damage.

There are several types of damage to spacecraft. These range from space debris, problems with the vacuum of space, various problems associated with the plasma environment, and various problems explicitly associated with the radiation environment. The radiation environment causes several types of hazards, but here we will look at one of the most common. This is the Sudden Event Upset (SEU), where, apparently, a single particle causes a piece of equipment to malfunction. Most ground controllers keep records of SEU's and these records are archived at the National Geophysical Data Center in Boulder.

An example of where SEU's occurred for the Topex/Poseidon spacecraft is given in Figure 4, for the period 1992-1998. This spacecraft

operated at an altitude of 1340 km, and the total geomagnetic field contours for this altitude are shown on the figure. As is characteristic, the places where the SEU occurred do not precisely fall within any single contour line. In this case most SEU's occurred where the geomagnetic field was less than 24,000 nT and the area enclosed by this contour is a somewhat different shape from the 24,000 nT contour at the Earth's surface.

Magnetograms from geomagnetic observatories near the SEU's were examined for the time when these SEU occurred but these magnetograms showed no unusual behavior. The planetary Ap index was studied to see if this index was large at the times of the SEU's, indicating disturbed conditions. Again the Ap's for those times did not differ significantly in their statistical distribution from the Ap's for all time during 1992-1998. These observations show SEU's bear little relation to general disturbed conditions.

There were 282 SEU's in or near the SAA over this 6 year period. On a statistical basis there were a few per week to a few per month, depending upon the solar cycle, and this frequency seem characteristic of spacecraft with radiation hardened components.

One of the clearest illustrations of how the radiation dose rate for humans is related to the SAA is given in paper by Badhwar (1997) and shown here in Figure 5. The dose rate as a function of latitude and longitude is shown for Skylab during December 1973 to January 1974 and for Mir during March 2-11, 1995. While this paper was written to show the change in location of the SAA over the 21.2 year period between the two data sets, it clearly defines the location of highest radiation dosages at the 400 km altitude of these two spacecraft. Mir's data shows that the peak in the dose curve extended from 10 S to 40 S and 5 W to 65 W in March of 1995. This approximately defines the 25,000 nT contour at 400 km altitude. However there are lesser, broader peaks in the Mir dose rates away from the SAA. These lesser peaks have not received much attention in the literature.

These studies show that the 25,000 nT contour is a critical one at altitudes up to 1000 km, as far as radiation damage to spacecraft or radiation hazards to humans is concerned.

#### **4. The Future of the South Atlantic Anomaly**

Precise predictions of the geomagnetic field, on almost any time scale, are well known to be impossible. However one can speak about average changes with a high probability of being correct. We will look at the historical record of past geomagnetic field changes and try to use that as a guide for estimating the most probable future field. Although measurements of magnetic inclination and declination extend back several centuries, the measurement of the geomagnetic intensity has only been possible since the time of Gauss, in 1833. Even at that time there were not enough measurements to draw accurate maps. One of the earliest world maps of the intensity was that for the year 1922 (Chapman and Bartels, 1940, p. 101) from records of the British Admiralty. If the map of secular change from the IGRF 95 coefficients (Figure 6) is used to extrapolate back from 1995 to 1922 the charts compare favorably in the South Atlantic. Sabaka, et al. (1997) have calculated secular variation for several epochs starting in the early parts of this century and, again, rates are similar to that of Figure 6.

In the literature several papers have reported changes in the center of the SAA from records from spacecraft (Badhwar et al., 1996; Badhwar, 1997; Golightly et al., 1994; Lauriente et al., 1995; Konradi et al., 1994). The more recent of these, which include larger data bases indicate a change of about 0.28 degrees W, 0.08 degrees N per year. If one uses the secular change coefficients in the IGRF 95 model, one obtains about the same values (0.20 degrees W, 0.02 degrees N per year) for the years 1973 - 1995. Since not all parts of the Earth have the same secular change the movement of the center of the SAA may be different from the movement of the SAA as a whole, as measured by the movement of the 25,000 nT contour.

Figure 6 shows that the greatest rate of secular change of the intensity is in the South Atlantic southwest of Cape Town where the rate is more than -100 nT/yr. There is a secondary area of rapid change of field strength in the North Atlantic where it exceeds -80 nT/yr. The IGRF 95 database carries a warning that it should not be extrapolated for more than a few years in the future if it is to be very accurate. This warning is justified because older historical data shows that the secular variation of directions of the field has been quite nonlinear in the past, for certain geomagnetic observatories, especially those in London, Hawaii, and in India but not for those around the South Atlantic. Here we are making the most reasonable estimate of the

future field by multiplying the changes shown in Figure 6 by the number of years of change and adding that to the 1995 field shown in Figure 1.

The process of making spherical harmonic models with a finite number of coefficients, such as the IGRF, necessitates smoothing over some values observed in making the model. Thus, if one wants to consider the future of the SAA, one should look carefully at the historical values which have been measured at geomagnetic observatories around the South Atlantic. The National Geophysical Data Center has records from 25 observatories around the South Atlantic, with 11 of them having annual mean records of 25 years or more. These 11 show rates of change similar to those shown in Figure 6, except that Hermanus, South Africa, and Syowa Base, Antarctica, show somewhat greater change.

Figure 7 shows annual means from five observatories with longer records. The dashed line with each record is a least square fit to the data and the slope of this line is indicated. The location of these observatories is shown in the upper left panel. All stations show a nearly linear decrease with time and all, excepting, as mentioned before, Hermanus (HER), show values like that shown by the IGRF 95 secular change (see upper left panel). *Monthly* mean values for 3 of these observatories are available from Institute Physique Globe, Paris. Although the scatter of values is greater for the monthly means than for the annual means, a least squares fit to the monthly mean values yields values very similar to those of the annual means.

The geological record of the paleomagnetic field provides little insight to changes in field strength on a time scale as short as 100 years. Creer et al. (1983) reported a paleomagnetic study of sediments from 3 lakes about 600 km northwest of the Trelew (TRW) observatory. The resolution of these measurements was not sufficient to yield information about the last few hundred years.

Using the IGRF 95 coefficients and their secular change the field was calculated and plotted for a number of years in the future. As an example Figure 8 is the field for the year 2100. It differs in several interesting and significant ways from the field for 1995 (Figure 1). The SAA, as defined by the 25,000 nT contour, covers a larger area of the South America, South Africa, and the South Atlantic. The SAA low has broken into two lows: one northwest of the present low of the SAA, and the other one southwest of Cape Town. In addition the low southwest of Cape Town is lower than the

low of 1995. The map for 2100 shows relatively little change for the highs south of Australia, in Siberia and in northern Canada.

Figure 9 illustrates field lines for the year 2100 along the Greenwich Meridian (0 degrees longitude), with mirror points for particles with various equatorial pitch angles (contrast with Figure 3). The Greenwich Meridian was chosen for this illustration because that is where the low southwest of Cape Town is located in 2100 (Figure 7). When this figure is compared to Figure 3 it is seen that the particles with smaller equatorial pitch angles can reach the top of the atmosphere in the region of this new low for the SAA where they could not in Figure 3.

## 5. Conclusions

If the geomagnetic secular variation continues for the next hundred years, as it has for the past hundred years, the South Atlantic Anomaly can be expected to greatly increase. There will likely be a smooth increase in the shape of the SAA, from year to year, from its present size to the shape indicated for the year 2100. The present focus of the SAA will move northwest and a new and deeper focus will appear southwest of Africa, near the Greenwich Meridian and 50 degrees south. Numerous manned and unmanned spacecraft will be orbiting through this area.

The consequence of this change for radiation damage in space will be to make the radiation damage more intense and for it to cover an area several times as large as present. More particles will be absorbed in the atmosphere and this could alter the overall number of particles in the radiation belts. Furthermore, since the longitudinal distribution of the field affects the ring current, that, too, may be altered and have a more global effect. A calculation of the change in the dip equator with time shows that by the year 2100 it will have moved north by 10 to 15 degrees in the North Atlantic, but will have little changed elsewhere.

The year 2100 was used to illustrate the change in the SAA with time but this same change can be extrapolated to even longer times. Using this extrapolation, the low in the field strength southwest of Cape Town will be reduced to zero in the year 2240, and the SAA would cover about half of the southern hemisphere at that time.

## Acknowledgements

The author acknowledges the support of NASA Goddard Space Flight Center.

## References

- Badhwar, Gautam D. 1997. Drift rate of the South Atlantic Anomaly, *Jour. Geophys. Res.*, 102, 2343-2349.
- Badhwar, G. D., et al. 1996. In flight radiation measurements on STS-60, *Radiat. Meas.*, 26, 17-34.
- Barton, C. E., and members of Working Group 8 1996. International geomagnetic reference field, 1995 revision, International Association of Geomagnetism and Aeronomy (IAGA) Division V, Working Group 8, *Geophys. J. Int.*, 125, 318-321.
- Creer, K. M., D. A. Valencio, A. M. Sinito, P. Tucholka and J. F. A. Vilas 1983. Geomagnetic secular variations 0-14000 yr BP as recorded by lake sediments from Argentina, *Geophys. J. R. astr. Soc.*, 74, 199-221.
- Chapman, S. and J. Bartels 1940. *Geomagnetism* (Oxford University Press, Oxford) p. 101.
- Fung, S. F. 1996. Recent Developments in the NASA Trapped Radiation Models, pp. 79-91, in *Radiation Belts: Models and standards*, Ed. By J. F. Lemaire, D. Heynderickx, and D. N. Baker, AGU Geophysical Monograph 97.
- Golightly, M.J., K. Hardy, and W. Quam 1994. Radiation dosimetry during U.S. Space Shuttle missions with the RME-III, *Radiat. Meas.*, 23, 25-42.
- Konradi, A., G.D. Badhwar, and L.A. Braby 1994. Recent space shuttle observations of the South Atlantic Anomaly and radiation belt models, *Adv. Space Res.*, 14(10), 911-921.

Laurients, M., A.L. Vampola, P. Inamti, and D. Bilitza 1995. Experimental validation of particle drift theories, paper presented at 32nd Informational Space Radiation Effects Conference, Int. of Electr. and Electron. Eng., Madison, Wis., July 17-21.

Sabaka, T.J., R.A. Langel, R. T. Baldwin, and J. A. Conrad 1997. The Geomagnetic Field 1900-1995, Including the Large-Scale field from Magnetospheric Sources and the NASA Candidate Models for the 1995 Revision of the IGRF, *J. Geomag. Geoelectr.* 49, 157-206.

## Figure Captions

Figure 1. Geomagnetic total field intensity, in nT, for 1995.0 based on IGRF 95. Contour interval 4000 nT.

Figure 2. Geomagnetic field lines leaving 20 S, 40 S, and 60 S for longitudes 40 W (left side) and 140 E (right side).

Figure 3. Height of geomagnetic field lines starting at 40 S, 30 S, and 20 S. The mirror points for particles with various equatorial pitch angles are marked, with the value of the equatorial pitch angle shown next to the point. These lines are along 60 W longitude and for the year 1995.0.

Figure 4. Places where Sudden Event Upsets occurred for the Topex/Poseidon spacecraft for the years 1992-1998. Contours of the geomagnetic total field intensity are shown for the altitude of the spacecraft (1340 km).

Figure 5. Dose rates for Mir and for Skylab as a function of latitude and of longitude (after Badhwar, 1997).

Figure 6. Secular variation of the total geomagnetic field intensity calculated from IGRF 95 coefficients (in nT/yr). Contour interval 20 nT/yr with negative values shown by dashed lines.

Figure 7. The change in the annual means of geomagnetic total field intensity for five geomagnetic observatories around the South Atlantic. Plots are shown for Vassouras, Brazil (VSS), Pilar, Argentina (PIL), Trelew, Argentina (TRW), Tsumba, Namibia (TSU), and Herman, South Africa (HER). The location of these observatories is shown in the panel at the upper left. Dotted lines, with accompanying numbers, show the least squares fit to a straight line for each observatory.

Figure 8. Geomagnetic total field intensity (in nT) for the year 2100, extrapolated from the year 1995.0 and using the IGRF 95 secular change coefficients. Contour interval 5000 nT.

Figure 9. Three geomagnetic field lines versus height for lines starting at 50 S, 40 S, and 30 S, along the Greenwich Meridian for the year 2100. Points along lines show where particles with a given pitch angle will mirror. The value of the equatorial pitch angle is shown next to the mirror position.

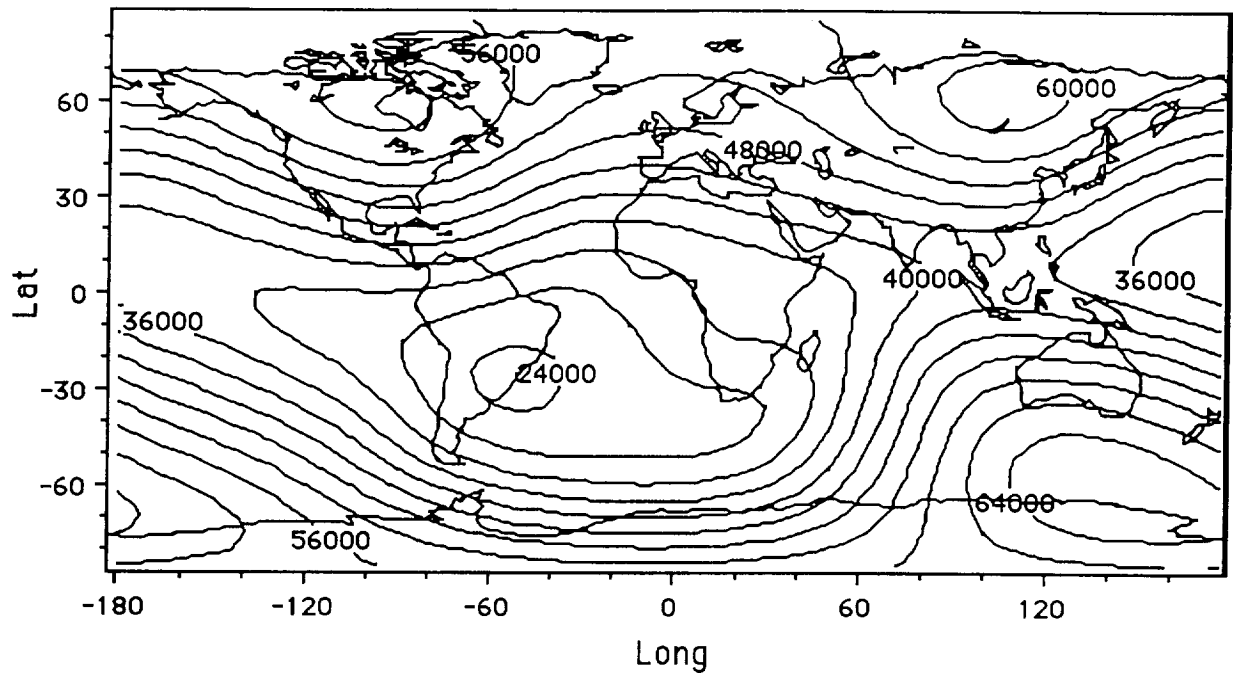


Fig. 1

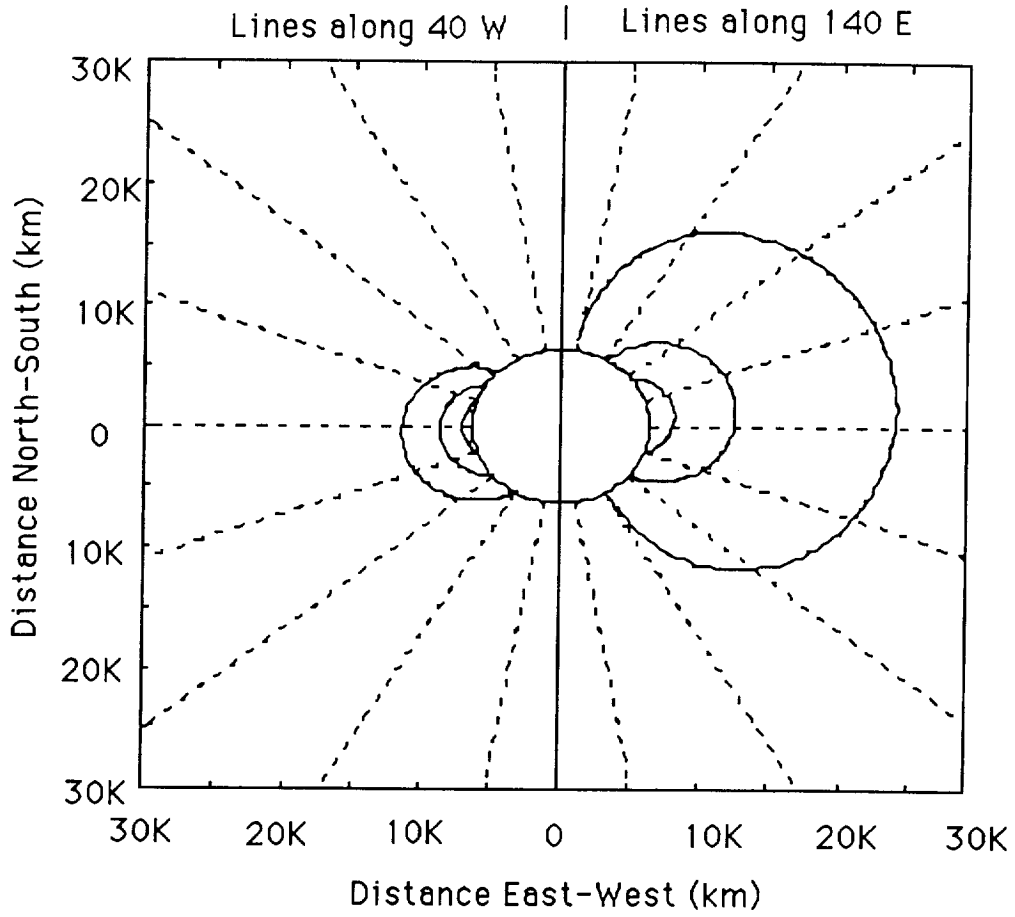


Fig. 2

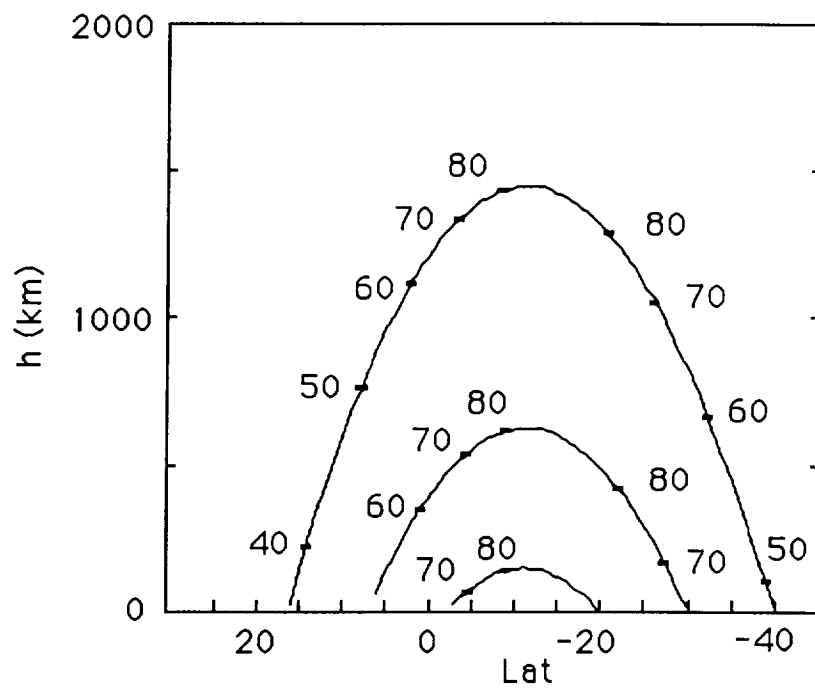


Fig. 3

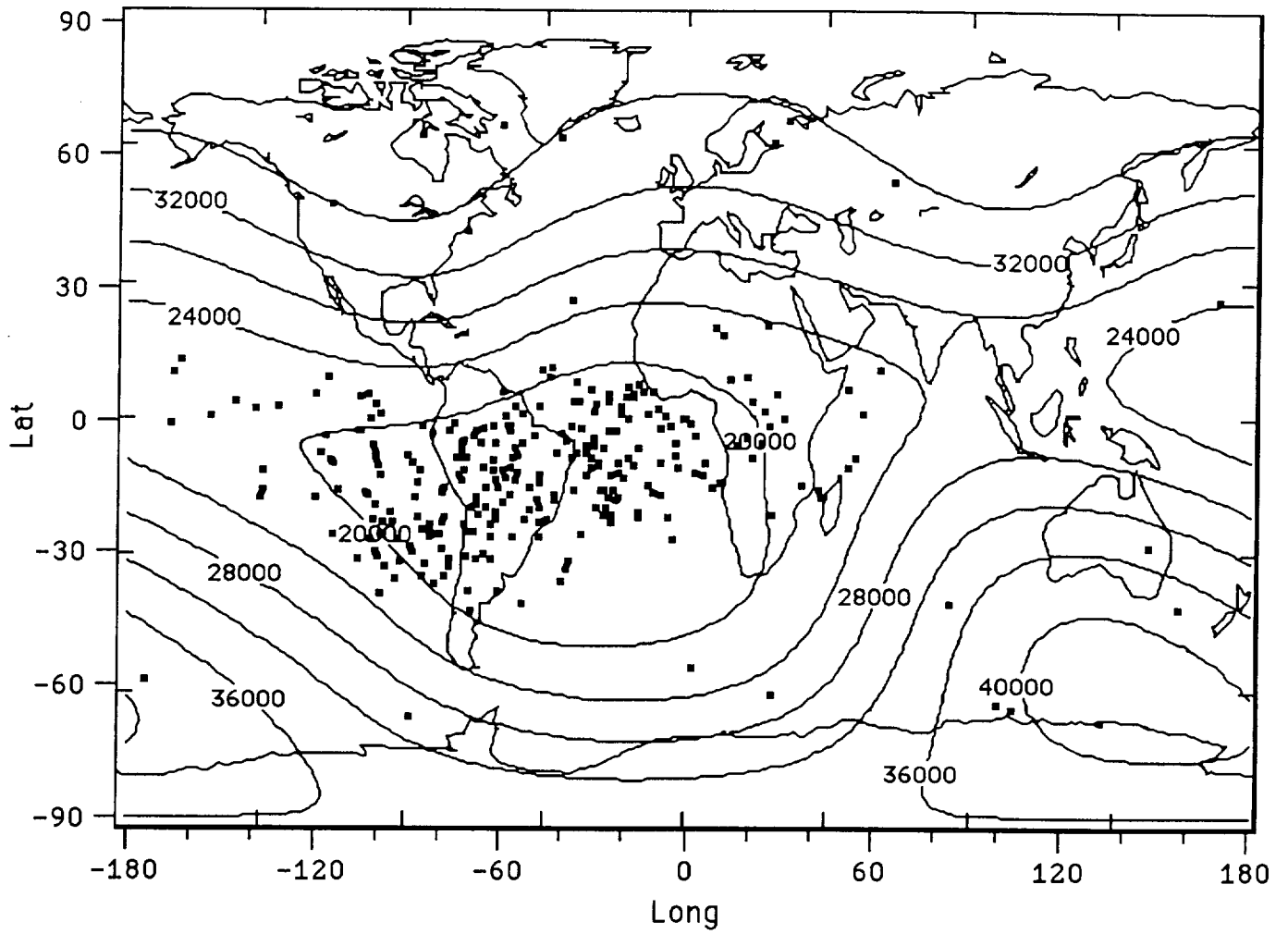


Fig. 4

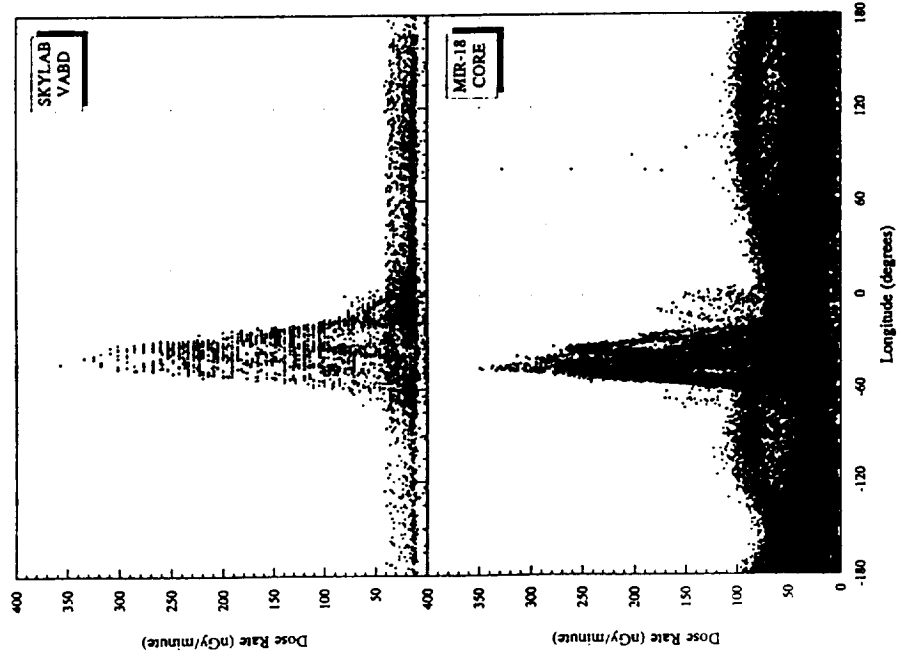
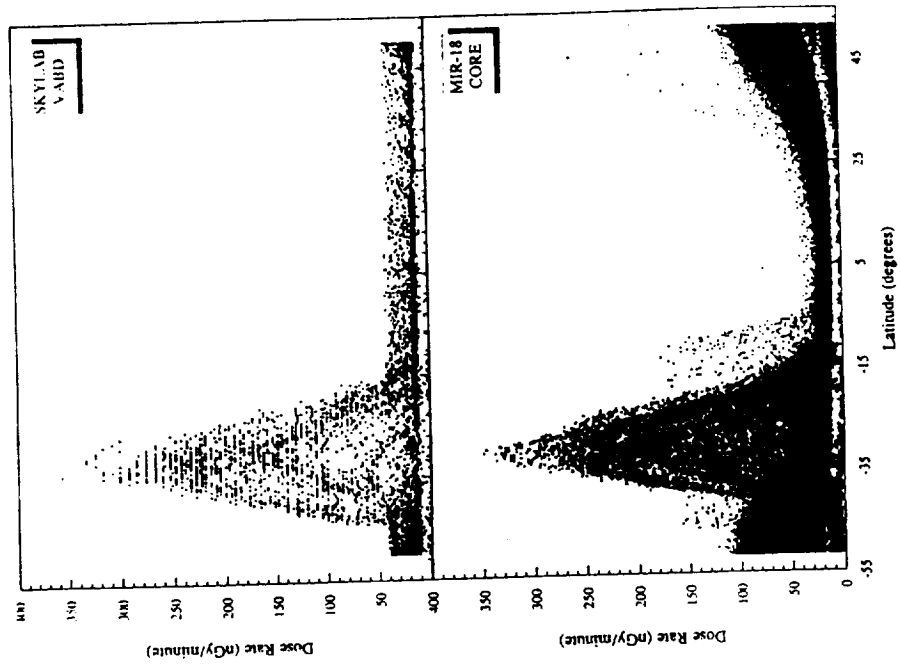


Fig. 5

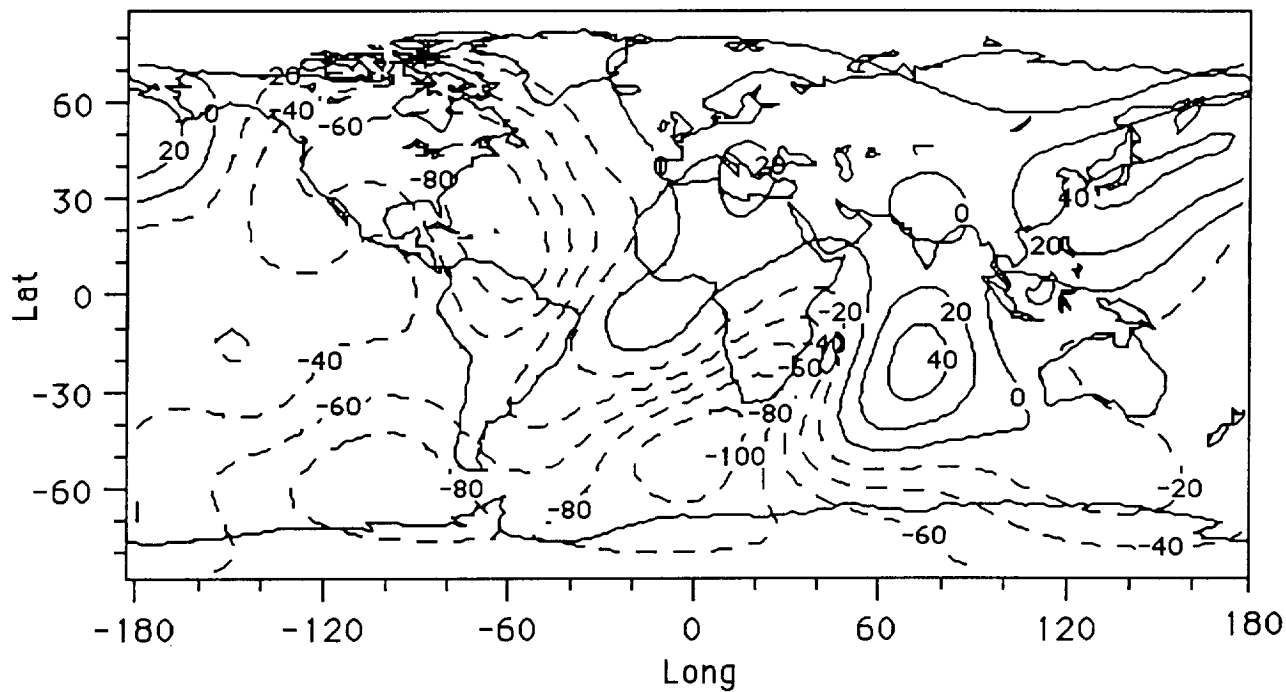


Fig. 6

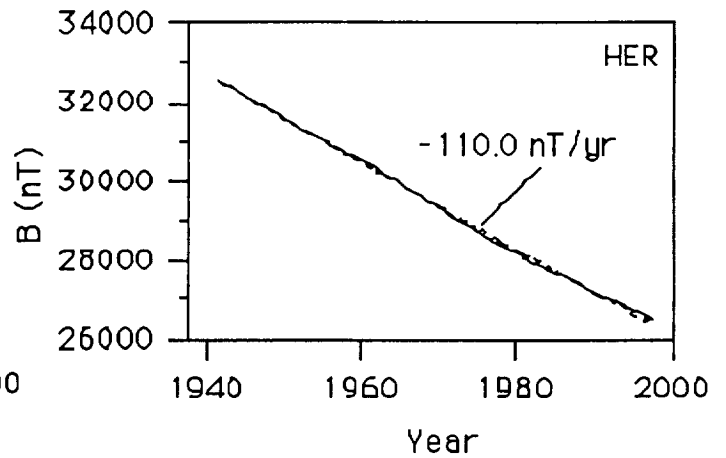
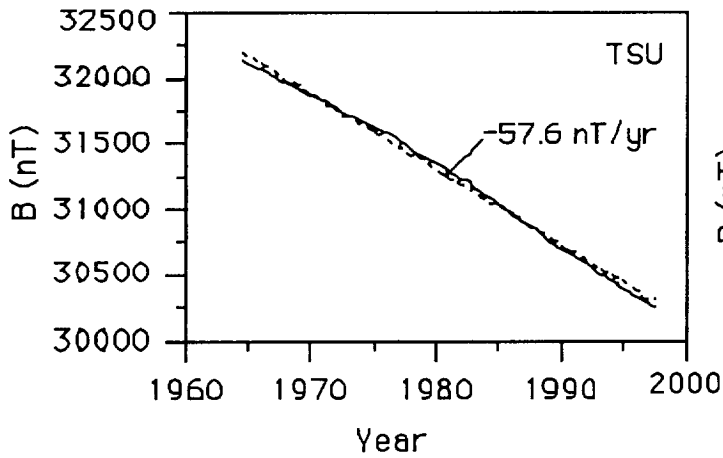
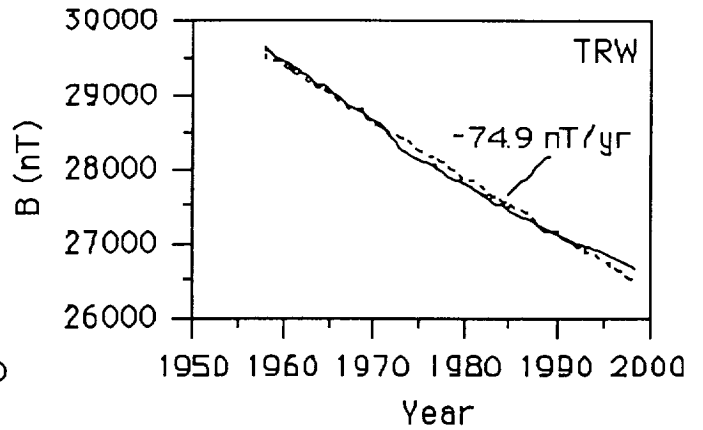
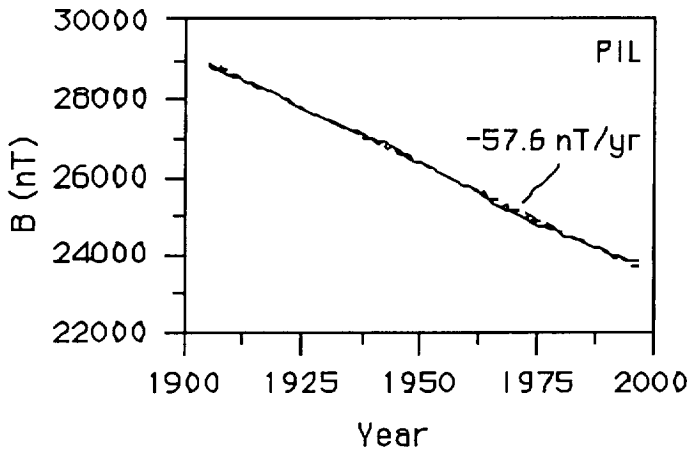
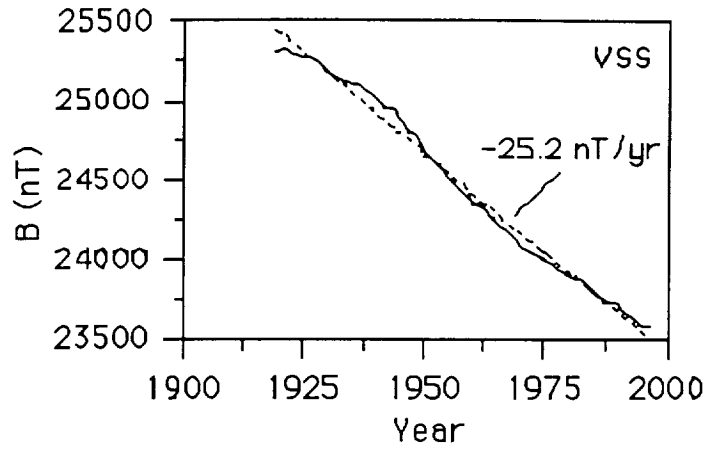
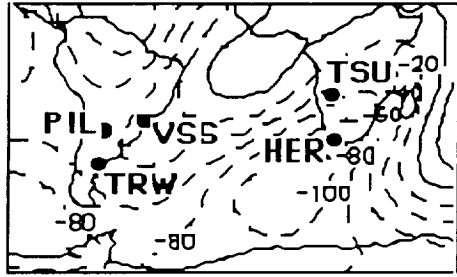


Fig. 7

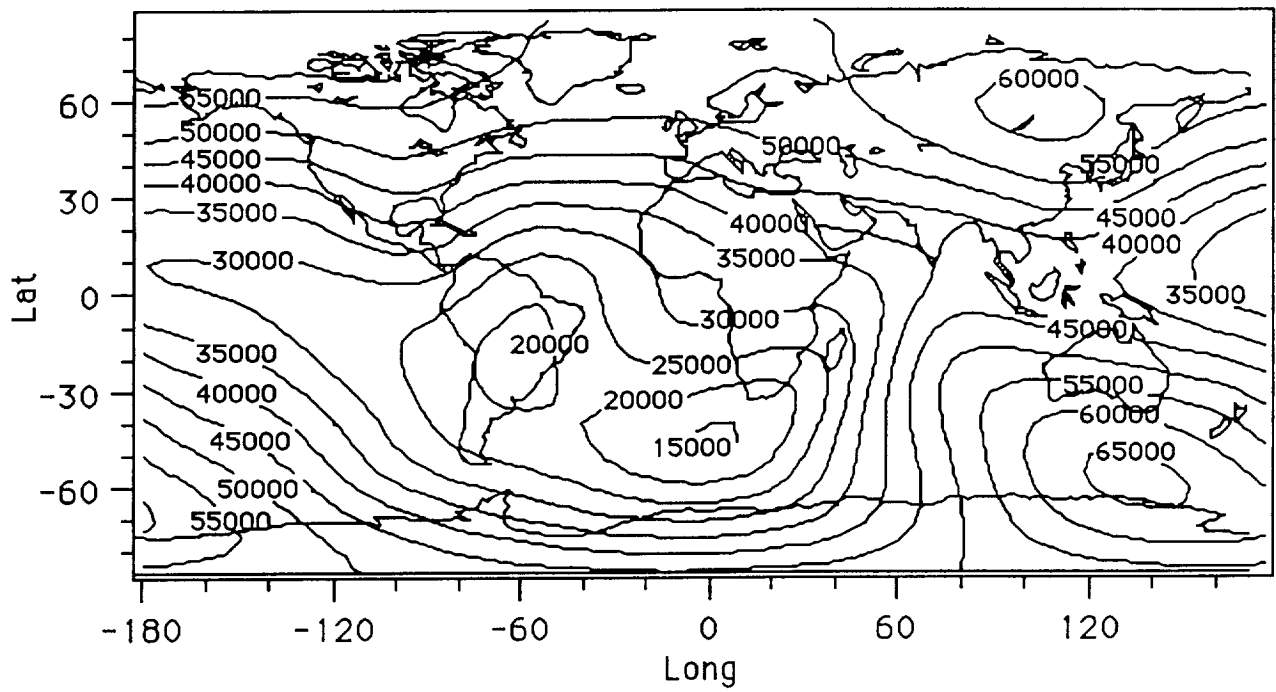


Fig. 8

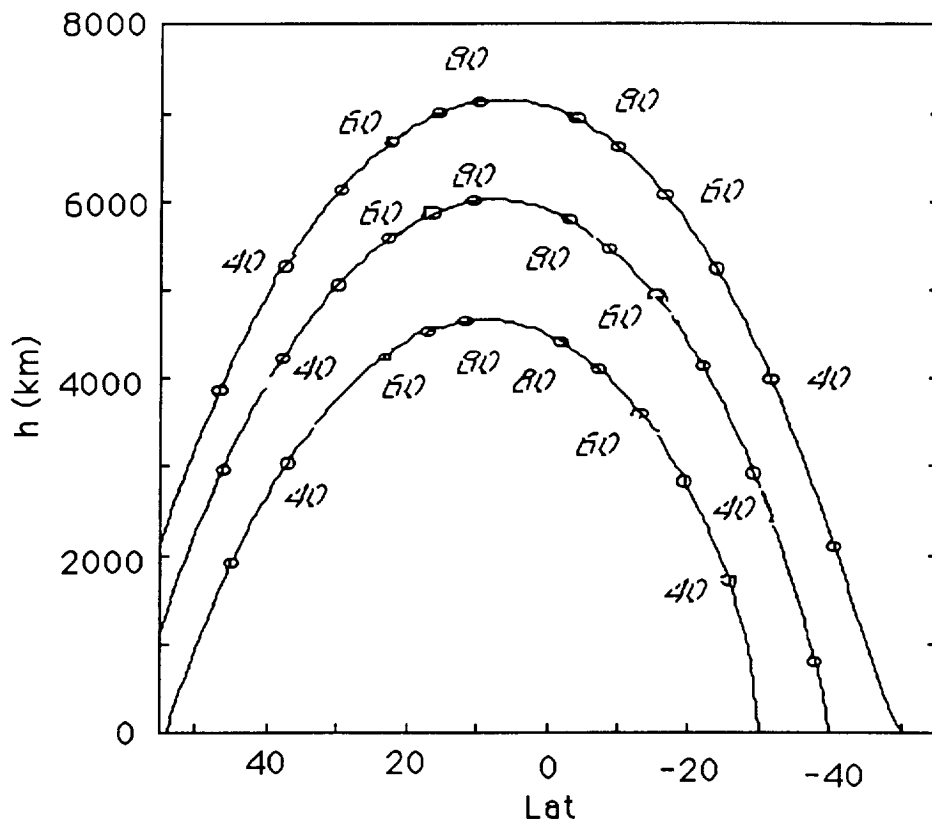


Fig. 9